

## Analysis of recipient mouse spleen tissues

### Fluorescence microscopy

Fluorescence microscopy was performed using an *Olympus Ax70* epifluorescence microscope (Olympus, Tokyo, Japan) fitted with a 16-bit cooled-CCD camera (Hanamatsu Photonics, KK, Japan) controlled by *AnalySIS® FIVE* software (Olympus). Photographs were taken using the 4×, 10×, 20× and 40× objective lenses (dry). Fluorescence illumination was performed using a mercury lamp and one of three filtersets optimised for the detection of DAPI, fluorescein or CMRA. Brightfield images were taken using the same microscope using standard lamp illumination.

Unscaled 12-bit TIFF images were acquired for each field using a defined exposure time optimised to restrict fluorescence signals within the dynamic range of the camera. For each field, multiple digital photographs were captured, recording:

- DAPI fluorescence – for estimating the total number of cells in the field;
- Fluorescein / *Alexa Fluor® 488* fluorescence – for the assessment of staining from biological assays; and,
- CMRA fluorescence – for identifying donor cells.

The DAPI fluorescence intensity was strong (from the DAPI nuclear counterstain incorporated into the anti-fade mounting medium), and was consistent across slides. An exposure time of 100 ms was used, except on rare occasions when the exposure time was lowered to 50 ms to keep the image brightness within the dynamic range of

the camera, e.g. where the fluorescence saturated the image intensity, usually towards the edge of a tissue section.

The intensity of fluorescein/*Alexa Fluor*® 488 stained cells, varied slightly:

- between cells in the same field/region/spleen section (due to different levels of enzymatic labelling/protein expression due to biological factors);
- between slides in the same experiment (due to variations in the number of cells contained in the cross-sectional area of the 5 µm spleen sections and slight variations in thickness between cut sections); and,
- between experiments conducted on different days (due to assay reagent batch variation, shelf-life of reagents and variations in exact timing depending on the number of slides being processed simultaneously).

After analysis of initial results using both fluorescence assays, it was determined that the cumulative variation in staining intensity due to all the factors outlined above, was acceptable, on the assumption that variation between replicates was due to the sources of error detailed above and not representative of true variation through the depth of the tissue. Given this observed consistency in the ‘average’ staining intensity, a constant exposure time of 1 second was used for imaging fluorescein or *Alexa Fluor*® 488 fluorescence for all experiments. In each of the experiments (except for acute X-ray irradiations), the fluorescent labelling of donor cells used the same concentration of the *CellTracker Orange*® CMRA dye and the same labelling time/conditions. As such, the fluorescence-labelled donor cells were imaged using a constant exposure time of 2 seconds.

All images were captured without gain adjustment in 12-bit resolution. For each image captured, the field number and filterset was recorded in the filename and the image was converted, without scaling, to an 8-bit image and saved in TIFF format. In cases where the field was identified at the time to be unsuitable, due to an obstructing particle, defect in the tissue section or difficulty achieving focus, another field was immediately chosen to replace the excluded field in order to maintain the total number of fields examined for each slide. In cases where a defect was not identified until after all the photographs had been captured for a slide, the defective field was excluded from further analysis without replacement. Images were analysed using *ImageJ v1.37a* software (National Institutes of Health, USA). Computerised image analysis was always conducted on the original 8-bit TIFF images; however, for observation, co-incidence of staining between fluorescence channels and archival purposes, a pseudo-coloured overlay of the images taken through each of the three filtersets was produced (using the *RGB Merge* function in ImageJ) and saved in compressed JPEG format.

### **Bystander screening methods**

One of the benefits of studying biological endpoints in frozen tissue sections is the retention of spatial information; one can determine the location of events in unirradiated bystander cells relative to each other, and to irradiated donor cells. This advantage, however, also poses the problem of how to quantify and express the biological information contained in staining of a section of a heterogeneous organ. The use of 5 µm frozen tissue sections (approximately one cell radius in thickness) allowed the three-dimensional architecture to be resolved into essentially two-dimensions; the analysis of a single plane of cells from a transverse section.

Hitherto, very few bystander experiments have been conducted in a three-dimensional complex tissue, and even those in a two-dimensional plane are often analysed *in toto* without retaining spatial information. As such, specific data pertaining to the distance bystander signals could travel *in vivo* or the sphere of influence of a single irradiated cell were not available. However, a limited number of *in vitro* studies were able to provide clues as to the regions of interest that should be examined.

Abscopal effects, where biological changes occur in unirradiated tissues distant or shielded from irradiated tissues, and the presence of clastogenic factors in serum from radiation-exposed individuals, both suggest wide-reaching, systemic communication from organ-to-organ. The direct comparison between abscopal/systemic effects and bystander effects as they pertain to radiation protection (i.e. sparse, individual exposed cells within an unexposed tissue) should be regarded with caution. Most abscopal effects are detected after very high dose irradiation of a tissue/region of the body which is likely to produce large amounts of cell death. In these cases, the propagation of effects (damage) is likely not a specific signal produced by the irradiated cells but the accumulation of toxic by-products from a tissue undergoing large-scale necrosis. The parallel is closest to ICCM transfer experiments, where the collective secretions/excretions of a large population of irradiated cells are added to a naïve unirradiated population in a bolus dose. Since the signalling pathways are potentially dissimilar, if they have a parallel at all, the expectation of organism-wide or inter-organ signal propagation from sparse, individual irradiated cells based on abscopal effects is not well founded.

Corollary data for organ-wide radiation responses however, is found in experiments where  $^{239}\text{Po}$  sources (of various sizes) were administered to the livers of Chinese hamsters. These experiments demonstrated that both the occurrence of chromosomal aberrations and the risk of liver cancer was dependent on the total radiation dose to the organ, regardless of whether the dose was diffused (as  $^{239}\text{Po}$ -citrate) or contained in  $^{239}\text{PoO}_2$  particles that delivered different non-uniform dose distributions (Brooks *et al.*, 1974; Brooks *et al.*, 1983). The authors concluded that the organ was responding to the radiation insult as a whole, an early precursor to the bystander phenomenon.

At the opposite end of the spectrum are the data where bystander effects in the unirradiated cells are dependent on direct cell–cell contact or intimate plating densities (Azzam *et al.*, 2001). These studies would suggest that bystander effects would be observed in a restricted, localised three-dimensional area surrounding irradiated cells. This proximal signalling hypothesis is complicated again by the potential for bystander cells to amplify and further propagate the signal to their own neighbouring unirradiated cells (Rugo *et al.*, 2007). The implication of GJIC in this contact-dependent phenomena has been confused by data which suggests that GJIC-deficient cell lines are still capable of producing the contact-dependent effect (Gerashchenko and Howell, 2003a).

Perhaps the best evidence to date comes from experiments using a charged-particle microbeam to irradiate a single plane in a three-dimensional human skin tissue reconstruction with analysis of apoptosis and micronuclei formation at various distances from the irradiated plane (Belyakov *et al.*, 2005). This pivotal work made the surprising conclusion that bystander effects could be detected at least 1 mm away

from the plane of irradiation (hundreds of cell diameters). Given that there were data to support both a global, organ-scale effect and a limited, local effect, it was decided to analyse the recipient tissues in two separate ways to allow both/either types to be observed.

### *Global screening*

The ‘global’ screening method refers to analysis of the frozen tissue sections from the recipient spleens using large fields of view (low magnification) chosen at random. The number of fields analysed and the number of recipient cells per field were chosen so as to give a large, representative sample of the entire section. This screening approach gives data averaged over the various cell-types and areas within the spleen regardless of the presence of irradiated or control donor cells. For each spleen section, at least 20 random fields (or as many as were possible) were photographed using the 20× objective lens giving a field size of 428 µm × 342 µm (*Figure 4.20* and *Figure 4.21*). If subtle, organ-wide responses were to occur, the global screening method surveys a sufficient number of cells to detect minor changes. A result of this strategy is that some fields will contain donor cells and others will not. Given that the 5 µm thick section only contains essentially a single depth layer of cells, the presence or absence of donor cells in the field of view is not a fair indication of whether donor cells are present before, or behind, the section along the Z-axis. Thus, the global screen is intended to represent this averaged response of the spleen tissue regardless of donor cell lodging. In addition, the global screening provides a random sampling of the spleen tissue from which the average density of lodged donor cells can be determined to calculate a donor cell lodging frequency.

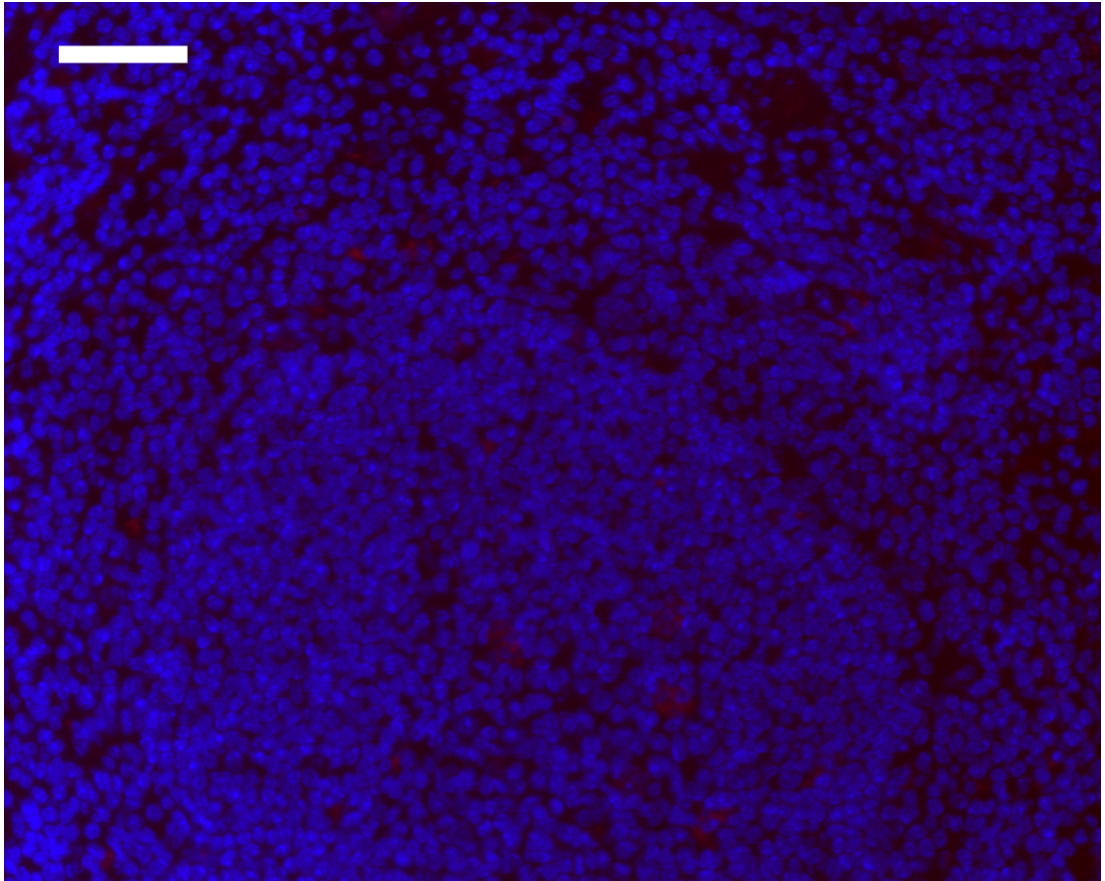


**Figure 4.20: Representative global field**

In the global screening method, stained spleen sections were photographed on a fluorescence microscope using a 20× objective lens giving a field size of 428  $\mu\text{m}$   $\times$  342  $\mu\text{m}$ , shown above. Non-overlapping fields were chosen randomly while viewing the DAPI channel (blue). Some fields contained lodged donor cells (red), others (like this field) did not. The fluorescence in the fluorescein channel (not shown) was photographed in the same fields to measure staining from biological assays. Scale bar shows 50  $\mu\text{m}$ .

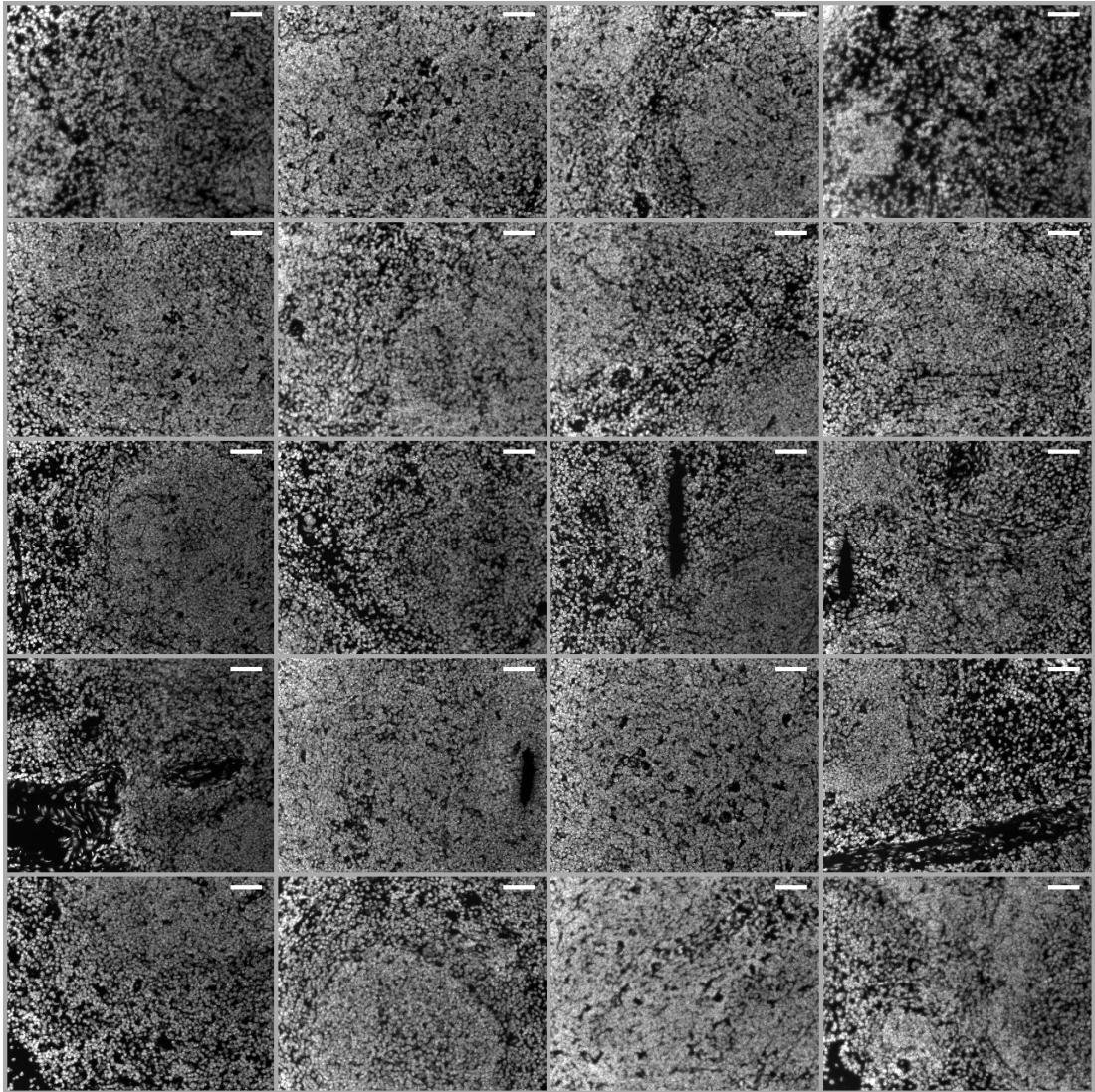


**Figure 4.21: Area surveyed in 20 representative global fields**

In the global screening method, stained spleen sections were photographed on a fluorescence microscope using a 20× objective lens giving a field size of 428  $\mu\text{m}$   $\times$  342  $\mu\text{m}$ . The photographs of the DAPI channel from twenty non-overlapping fields (from a single spleen section) are shown above. Scale bars show 50  $\mu\text{m}$ .

### *Local screening*

In contrast to the global screen, the local screening method was designed to examine selectively the area immediately surrounding lodged donor cells. In the local screening method, all fields containing at least one donor cell (up to a maximum of 25 fields per section) (*Figure 4.22*) were photographed using the 40× objective lens giving a field size of 212 µm × 170 µm (*Figure 4.23*). With placement of a single donor cell in the centre of the field, the bystander cells analysed are within a radius of 85 µm up to 136 µm, with 81% of cells within 100 µm from the centre (*Figure 4.23*). Where multiple donor cells were clustered together such that the fields of view overlapped, the group of cells were photographed in a single field with the centroid of the shape formed by the donor cells placed in the centre of the field. In such cases, the proportion of recipient cells within 100 µm of a donor cell approached 100%.

### **Autoradiography**

To detect the radioactivity in the radiolabelled donor cells lodged within the spleen, tissue sections were processed for autoradiography, either directly on fixed tissues, or following staining for bystander endpoints.

#### ***Method:***

Coverslips were removed from pre-stained slides by briefly soaking in PBS; unstained slides were rinsed in PBS. Slides were then dried, dehydrated through 70%, 90% then 100% ethanol and allowed to dry again. Slides were then processed for autoradiography as described earlier.

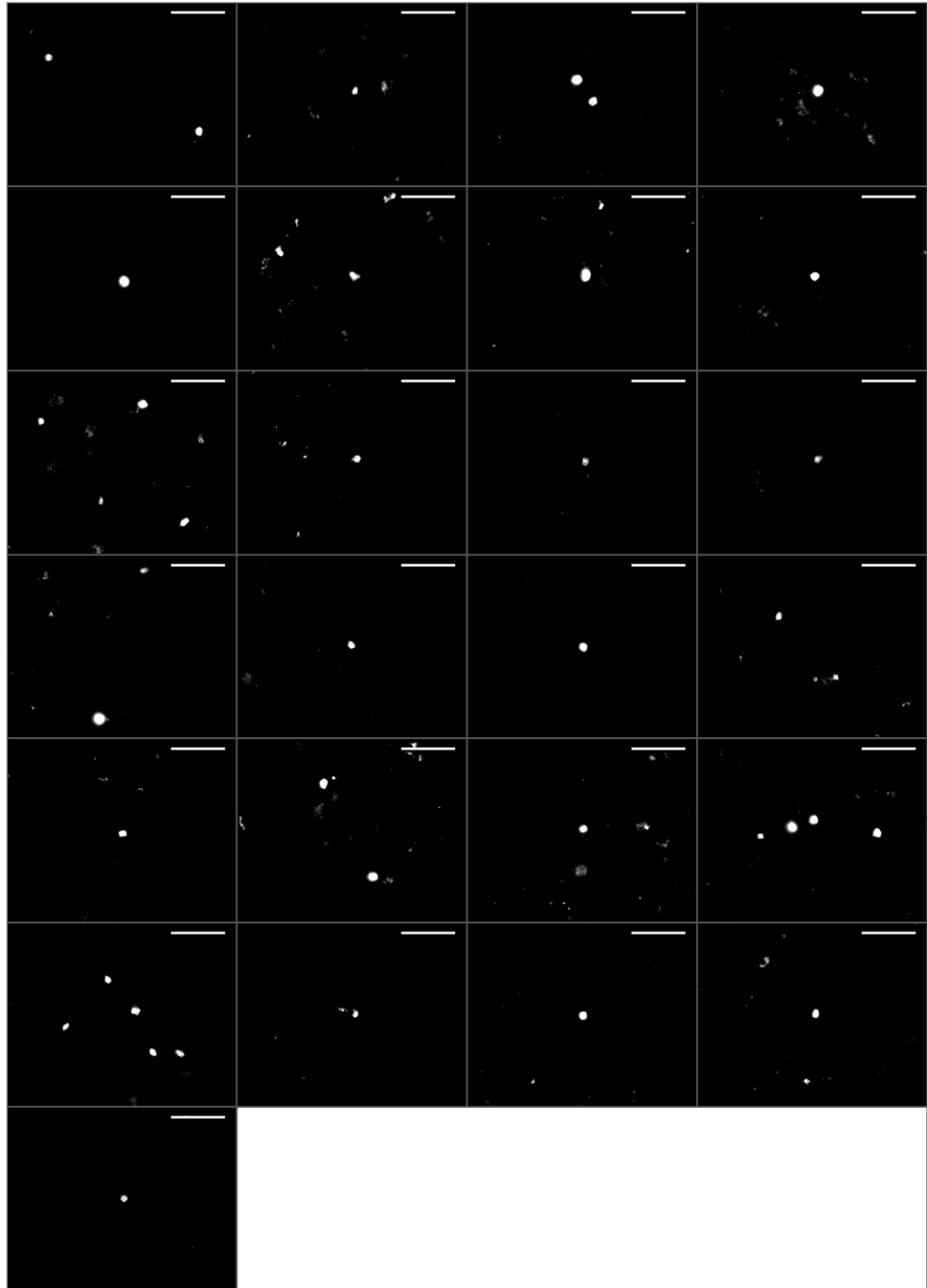


**Figure 4.22: Donor cells surveyed in 25 representative local fields**

In the local screening method, lodged donor cells were identified in stained spleen sections using the filterset for CMRA fluorescence, and the field of view was centred on the donor cell(s). Each field containing at least one donor cell was included up to a maximum of 25 fields. The photographs of the CMRA channel from twenty-five fields (from a single spleen section) are shown above. Scale bars show 50  $\mu\text{m}$ .

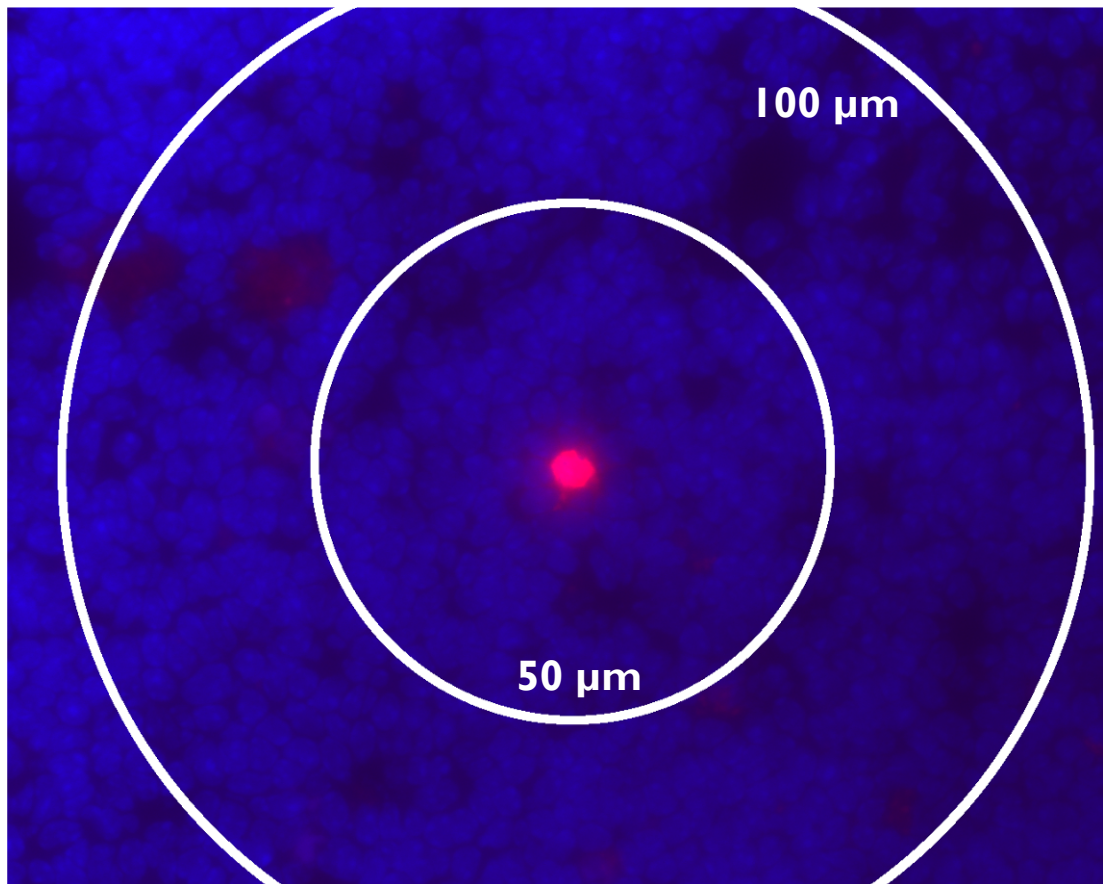


**Figure 4.23: Region included in the area around donor cells in a representative local field**

In the local screening method, lodged donor cells were identified in stained spleen sections using the filterset for CMRA fluorescence, and the field of view was centred on the donor cell(s). The DAPI-counterstained nuclei (blue) and CMRA-positive donor cells (red) were photographed using a 40× objective lens giving a field size of 212 μm × 170 μm, shown above. The fluorescence in the fluorescein channel (not shown) was photographed in the same fields to measure staining from biological assays. The inner circle shows the area included in a 50 μm radius around the donor cell, the outer circle marks 100 μm radius. The area within 100 μm of the donor cell includes 81% of the field.